

# Electrical conduction and optical properties of doped silicon-on-insulator photonic crystals

Paolo Cardile,<sup>1,3,4,a)</sup> Giorgia Franzò,<sup>4</sup> Roberto Lo Savio,<sup>5</sup> Matteo Galli,<sup>5</sup> Thomas F. Krauss,<sup>1</sup> Francesco Priolo,<sup>2,3,4</sup> and Liam O' Faolain<sup>1</sup>

<sup>1</sup>*SUPA, School of Physics and Astronomy, University of St. Andrews, North Haugh, KY16 9SS St. Andrews, United Kingdom*

<sup>2</sup>*Dipartimento di Fisica e Astronomia, Università di Catania, via S. Sofia 64, 95123 Catania, Italy*

<sup>3</sup>*Scuola Superiore di Catania, via Valdisavoia 9, 95123 Catania, Italy*

<sup>4</sup>*CNR-IMM MATIS, via S. Sofia 64, 95123 Catania, Italy*

<sup>5</sup>*Dipartimento di Fisica "A. Volta," Università di Pavia, via Bassi 6, 27100 Pavia, Italy*

(Received 25 February 2011; accepted 28 March 2011; published online 17 May 2011)

We investigate the electrical properties of silicon-on-insulator (SOI) photonic crystals as a function of both doping level and air filling factor. The resistance trends can be clearly explained by the presence of a depletion region around the sidewalls of the holes that is caused by band pinning at the surface. To understand the trade-off between the carrier transport and the optical losses due to free electrons in the doped SOI, we also measured the resonant modes of L3 photonic crystal nanocavities and found that surprisingly high doping levels, up to  $10^{18}/\text{cm}^3$ , are acceptable for practical devices with Q factors as high as  $4 \times 10^4$ . © 2011 American Institute of Physics. [doi:10.1063/1.3580613]

Two-dimensional photonic crystals (PhC) (Ref. 1) and cavities have been widely studied for many applications in quantum electrodynamics,<sup>2</sup> nonlinear enhancement,<sup>3</sup> and low threshold lasing.<sup>4,5</sup> Carrier injection often plays a crucial role, for example, in modulators<sup>6</sup> and lasers.<sup>7</sup> However, despite its importance, only a few studies on carrier transport through a photonic crystal have been reported in literature.<sup>8,9</sup> An accurate study is necessary to provide an understanding of the specific lattice design on the electrical behavior of a PhC electrical device. Another important issue is the trade-off between the electrical properties, e.g., the resistance, and the optical properties of PhC, e.g., the cavity Q factor. In this letter, we address these problems for silicon, one of the most important platforms in use for optoelectronic devices.

To carry out this study,  $p^+p-p^+$  like devices were fabricated on a SOITEC silicon-on-insulator (SOI) wafer ( $\rho \sim 1-10 \Omega \text{ cm}$ , corresponding to a p-type doping level of  $\sim 1 \times 10^{15} \text{ cm}^{-3}$ ), with a 220 nm thick silicon layer on a 2  $\mu\text{m}$  thick buried oxide layer. Boron implantations were used for all doping steps, using a 400 kV HVEE Ion Implanter. Multiple B implantations, at different energies and doses, were performed to provide the background doping (the p region), thus allowing us to investigate a doping range spanning three orders of magnitude (between  $\sim 1 \times 10^{15}$  and  $1 \times 10^{18} \text{ B/cm}^3$ ). Resistive contacts were formed on highly doped  $p^+$  regions with a concentration of  $1 \times 10^{19} \text{ B/cm}^3$ . After implantation, a rapid thermal treatment at 1000 °C for 30 s in  $\text{N}_2$  was carried out in order to recover the damage and activate the dopant.<sup>10</sup>

The PhC patterns were realized in the p region of the devices using electron beam lithography in a 400 nm layer of ZEP-520A (Zeon Chemicals). This pattern was transferred to the silicon layer by reactive ion etching with a  $\text{SF}_6:\text{CHF}_3 = 1:1$  gas mixture, etching through the entire silicon layer.

Finally, aluminum contacts were deposited. The complete structure is shown in Fig. 1.

We also etched isolating trenches around the device in order to avoid current leakage and to ensure that the electron flow is confined to the photonic crystal as the only possible conductive path. The photonic crystals occupy an area  $\sim 4.5 \mu\text{m}$  long and  $\sim 100 \mu\text{m}$  wide and the  $p^+$  pads are separated by  $\sim 10 \mu\text{m}$ . The geometrical filling factor of the photonic crystals  $f = (2\pi/\sqrt{3}) \cdot (r/a)^2$  was varied by changing the radius of the holes  $r$  and keeping the lattice parameter fixed at  $a = 400 \text{ nm}$ .

As expected, the measured I-V curves are linear and symmetric (not shown). The measured resistance is given by the slope of the I-V curve and includes the resistance of the PhC, the unpatterned silicon, and the contacts (about 300  $\Omega$ ). Devices without photonic crystals were included for reference and the key data are presented in Fig. 2. For

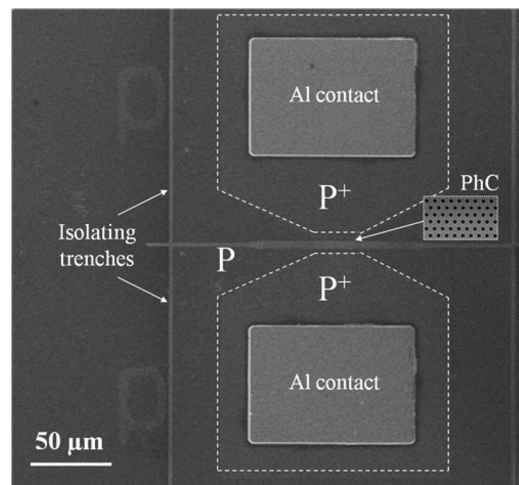


FIG. 1. SEM image of the  $p^+p-p^+$  device, showing all the doped sections, the zoomed-in view of the photonic crystals, the isolating trenches dug around the structure and the Al contacts.

<sup>a)</sup>Electronic mail: paolo.cardile@ct.infn.it.

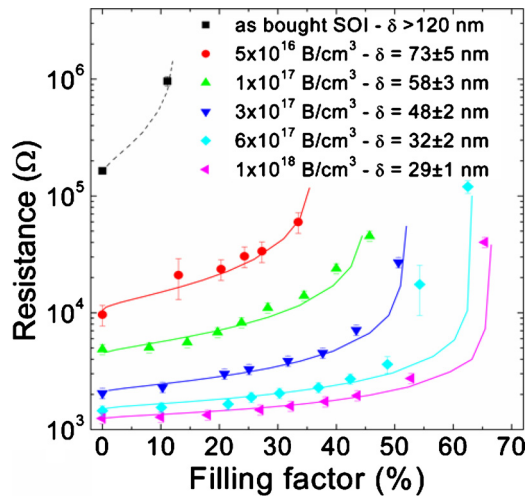


FIG. 2. (Color online) Total devices resistance (data points) as a function of both the background doping and the PhC air filling factor. The zero filling factor datapoint refers to the reference device, i.e., the one without any photonic crystal. The curves are obtained with COMSOL simulations and the extrapolated depletion region  $\delta$  is indicated for each doping level, with the exception of the as-bought SOI (dashed line), for which there was insufficient datapoints.

a given filling factor, the resistance decreases by more than two orders of magnitude from the as-bought SOI ( $\sim 1 \times 10^{15}$  B/cm<sup>3</sup>) to the highest boron concentration ( $1 \times 10^{18}$  B/cm<sup>3</sup>), as a result of the decreasing resistivity. The resistance then increases dramatically with increasing  $f$ , as the volume of material available for conduction is reduced.

Naively, one would expect the curves to diverge (i.e., resistance going to infinity) when the holes touch one another ( $f \approx 90\%$ ) as the conduction path is pinched off at this point. This is clearly not the case, and the curves in Fig. 2 show that the point of divergence strongly depends on the background doping level. For low doping concentration ( $5 \times 10^{16}$  B/cm<sup>3</sup>) the resistance starts to increase for filling factors as small as  $f \approx 30\%$ , while for a relatively high doping concentration ( $1 \times 10^{18}$  B/cm<sup>3</sup>) the resistance stays low until approximately  $f \approx 60\%$ . This suggests that the effective electrical size of the holes is larger than their physical size and that it strongly depends on the doping concentration. We have matched the experimental data by adding an additional electrically isolated region of dimension  $\delta$ , whose value is also a function of doping. The data points have then been fitted by using a COMSOL<sup>SM</sup> simulation for each doping density, shown as continuous lines in Fig. 2. The value of  $\delta$  decreases from 73 nm (for  $5 \times 10^{16}$  B/cm<sup>3</sup>) to 29 nm (for  $1 \times 10^{18}$  B/cm<sup>3</sup>).

A question arises on the physical meaning of  $\delta$ . In fact, dry etching is a severe physical process that introduces defects and deeply modifies the surface potential at the holes. These defects can pin the Fermi level position at the surface exactly in the middle of the gap, hence producing a depletion region  $\Delta$  around the holes. This depletion region can be calculated from Poisson's equation ( $\Delta = \sqrt{2\epsilon_r\epsilon_0\Phi_i/eN_A}$ , with  $\Phi_i$  being the internal potential of the semiconductor and  $N_A$  the boron concentration) and compared with the  $\delta$  obtained by the best fits of the experimental data. For example, for a doping density of  $N_A = 3 \times 10^{17}$  B/cm<sup>3</sup>, in the middle of the range investigated,  $\delta = 48 \pm 2$  nm, while  $\Delta = 44$  nm, so they

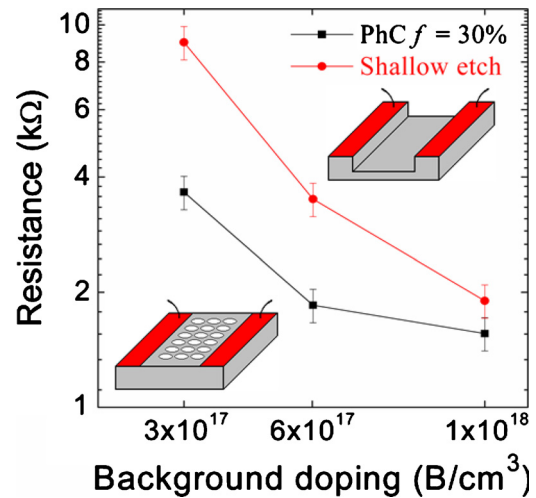


FIG. 3. (Color online) Resistance vs doping density, comparison of PhC vs shallow etched trench. The device length is  $4.5 \mu\text{m}$  in both cases. For a typical air filling factor of  $f = 30\%$ , the resistance through a photonic crystal section is considerably lower. The device layer is 220 nm Si in both cases, etched down to 85 nm for the trench.

are in good agreement, demonstrating that indeed the enlargement in the electrical size of the holes is produced by band pinning (similar agreement was found for the other doping levels). A depletion region also exists for the top surface of the SOI, but that surface has not been exposed to a dry etching process, so the band pinning effect there is much weaker. Note that a similar depletion region around etched holes has already been observed in indium phosphide<sup>8</sup> and gallium arsenide<sup>9</sup> photonic crystal devices.

An interesting comparison can now be made with the electrical properties of a shallow etched region, as both photonic crystals and shallow etching can be used to confine light. Which one of the two methods is better from an electrical point of view has not yet been made clear. Therefore we have investigated the resistance of shallow trenches (etch depth = 135 nm, i.e., 85 nm remaining, and different lengths) typically used to define rib waveguide based ring resonators.<sup>11</sup> The values of  $\delta$  were determined from the slope of a resistance-width plot, but  $\delta$  now refers to the surface rather than the sidewall depletion layer. As shown in Fig. 3, the resistance of a photonic crystal layer ( $f = 30\%$ ), is consistently lower than that of a shallow etched trench of the same length. This demonstrates both that the depletion layer needs to be considered for any type of electrically active nanophotonic device and that PhC are characterized by a lower resistance per length values.

It is clear from the electrical characterization that increasing doping concentration reduces the resistivity. A high doping level also increases the optical losses, however, so there is a clear trade-off between electrical and optical properties of doped devices. Therefore, in the second part of this letter, we explore the effect of doping on the cavity losses by measuring their Q factor. For each background doping level, we realized L3 nanocavities, with a lattice parameter of 420 nm and  $f \approx 28\%$  that operate at wavelengths around  $1.55 \mu\text{m}$ . The cavities were realized as air-bridges (while the electrical characterization was done on-substrate) and the far-field pattern of the cavities was optimized as discussed in Ref. 12, using hole enlargements of 0, +3 and +9 nm to improve the out-of-plane coupling efficiency. This

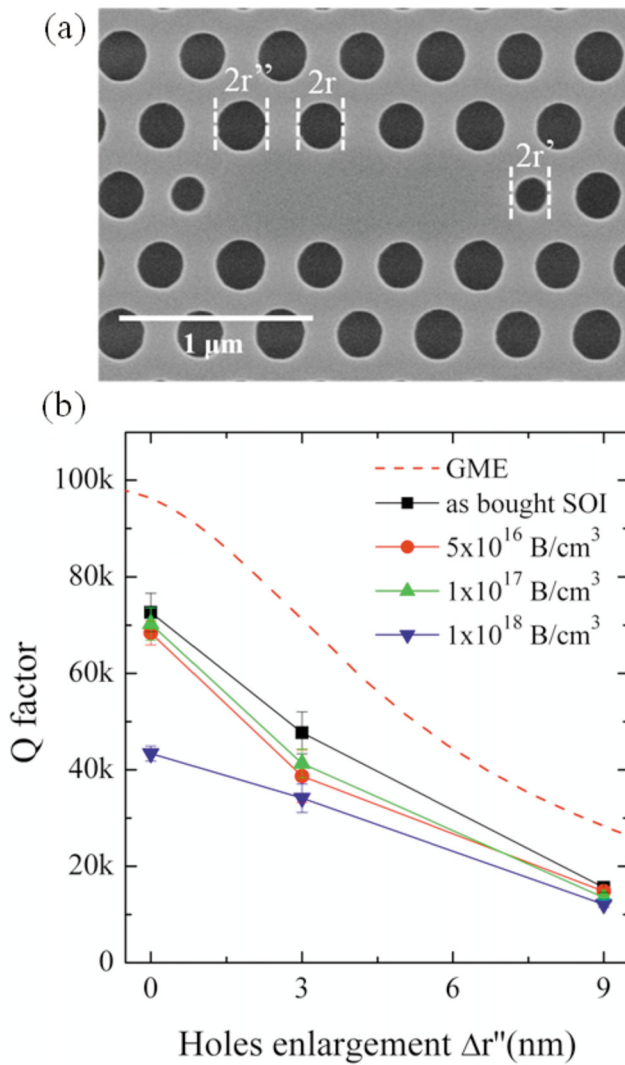


FIG. 4. (Color online) (a) SEM image of a L3 cavity; the radius of the holes ( $r$ ), the enlarged holes ( $r''$ ) for far-field and the side holes ( $r'$ ) for gentle confinement are evidenced. (b) Measured Q factor of L3 cavities as a function of the holes enlargement  $\Delta r''$  and different background doping levels. A GME calculation is also reported (dashed line).

hole enlargement ( $\Delta r'' = r'' - r$ ) is clearly visible in the SEM image shown in Fig. 4(a), in which a cavity is pictured in detail. The end holes at the sides of the cavities were reduced in radius by  $(r' - r)/a = 0.06$  and shifted outwards by  $\Delta x/a = 0.16$  to implement the gentle confinement effect, which allows the achievement of very high Q factors.<sup>13</sup> We measured the Q factors of the cavities using resonant scattering measurements.<sup>14</sup> The experimental points are shown in Fig. 4(b) for four different doping levels as a function of the hole enlargement parameter  $\Delta r''$  and are compared with calculations using the guided-mode expansion (GME) method.<sup>15</sup> Each experimental point has been obtained by measuring five cavities for each sample; the error bars are also shown and are due to statistics. For boron concentrations up to  $1 \times 10^{17}$  B/cm<sup>3</sup> the Q factors are little effected by doping, and display the same trend as the theoretical curve, i.e., they drop steadily from the maximum value of 75k (theoretical

value  $\sim 100k$ ) with increasing the far-field optimization, i.e., the  $\Delta r''$  parameter. As the doping level is raised to  $1 \times 10^{18}$  B/cm<sup>3</sup>, a more pronounced reduction in the Q factor is observed for the cavity without far-field optimization ( $\Delta r'' = 0$  nm), which nevertheless keeps at the remarkable value of 40k. We also notice that for the case of  $\Delta r'' = +9$  nm, the Q factor ( $\sim 15k$ ) does not change significantly even for the highest boron concentration. For this design, the coupling efficiency is approx 30% (Ref. 14) which means that the coupling loss is much higher than the absorption loss introduced by the doping.

In summary, we have characterized the effects of doping on the electrical and optical properties of silicon photonic crystals. We have clearly shown the effect of the surface depletion region around the etched holes, which is due to Fermi level pinning. We have also demonstrated that it is possible to have a more than two orders of magnitude improvement of the electrical conductivity of SOI, by relatively heavy ( $1 \times 10^{18}$  B/cm<sup>3</sup>) doping. Surprisingly, this reduces the experimentally measured unloaded Q of L3 PhC cavities by less than a factor of 2 and has an almost negligible effect on designs which exhibit high coupling efficiencies. We have thus provided useful guidelines for the design of electrically pumped photonic crystal devices.

The authors are grateful to D. Gerace and L. C. Andreani for GME calculations and to S. Tati, C. Percolla, and S. Balfour for technical support. This work was partially supported by ERA-NET NanoSci-E+ LECSIN project. Liam O'Faolain and Thomas F. Krauss acknowledge support from the EPSRC "UK Silicon Photonics" project.

<sup>1</sup>T. F. Krauss, R. M. De La Rue, and S. Brand, *Nature (London)* **383**, 699 (1996).

<sup>2</sup>T. Yoshie, A. Sherer, J. Hendrickson, G. Khitrova, H. M. Gibbs, G. Rupper, C. Ell, O. B. Shchekin, and D. G. Deppe, *Nature (London)* **432**, 200 (2004).

<sup>3</sup>M. Galli, D. Gerace, K. Welna, T. F. Krauss, L. O'Faolain, G. Guizzetti, and L. C. Andreani, *Opt. Express* **18**, 26613 (2010).

<sup>4</sup>M. Nomura, S. Iwamoto, M. Nishioka, S. Ishida, and I. Arakawa, *Appl. Phys. Lett.* **89**, 161111 (2006).

<sup>5</sup>S. Strauf, K. Hennessy, M. T. Rakher, Y.-S. Choi, A. Badolato, L. C. Andreani, E. L. Hu, P. M. Petroff, and D. Bouwmeester, *Phys. Rev. Lett.* **96**, 127404 (2006).

<sup>6</sup>T. Tanabe, K. Nishiguchi, E. Kuramochi, and M. Notomi, *Opt. Express* **17**, 22505 (2009).

<sup>7</sup>H. Park, S. Kim, S. Kwon, Y. Ju, J. Yang, J. Baek, S. Kim, and Y. Lee, *Science* **305**, 1444 (2004).

<sup>8</sup>A. Berrier, M. Mulot, G. Malm, M. Östling, and S. Anand, *J. Appl. Phys.* **101**, 123101 (2007).

<sup>9</sup>B. Ellis, T. Sarmiento, M. Mayer, B. Zhang, J. Harris, E. Haller, and J. Vuckovic, *Appl. Phys. Lett.* **96**, 181103 (2010).

<sup>10</sup>F. Priolo, G. Mannino, M. Micciché, V. Privitera, E. Napolitani, and A. Carnera, *Appl. Phys. Lett.* **72**, 3011 (1998).

<sup>11</sup>F. Y. Gardes, A. Brimont, P. Sanchis, G. Rasigade, D. Marris-Morini, L. O'Faolain, F. Dong, J. M. Fedeli, P. Dumon, L. Vivien, T. F. Krauss, G. T. Reed, and J. Martí, *Opt. Express* **17**, 21986 (2009).

<sup>12</sup>S. L. Portalupi, M. Galli, C. Reardon, T. F. Krauss, L. O'Faolain, L. C. Andreani, and D. Gerace, *Opt. Express* **18**, 16064 (2010).

<sup>13</sup>Y. Akahane, T. Asano, B.-S. Song, and S. Noda, *Nature (London)* **425**, 944 (2003).

<sup>14</sup>M. Galli, S. Portalupi, M. Belotti, L. C. Andreani, L. O'Faolain, and T. F. Krauss, *Appl. Phys. Lett.* **94**, 071101 (2009).

<sup>15</sup>L. C. Andreani and D. Gerace, *Phys. Rev. B* **73**, 235114 (2006).